RSC Advances

ROYAL SOCIETY OF CHEMISTRY

www.rsc.org/advances

Topotactic synthesis and photocatalytic performance of one-dimensional $ZnNb_2O_6$ nanostructures and one-dimensional $ZnNb_2O_6/KNbO_3$ hetero-nanostructures

Xingang Kong[ad*], Zhanglin Guo[a], Puhong Wen[b], Liyun Cao[a], Jianfeng Huang[a], Cuiyan Li[a], Jie Fei[a], Fen Wang[a], Qi Feng[c]

[a] School of Materials Science and Engineering, Shaanxi University of Science and Technology, Weiyang, Xi'an, Shaanxi 710021, PR China

[b] Department of Chemistry and Chemical Engineering, Baoji University of Arts and Science, 1 Gaoxin Road, Baoji, Shaanxi 721013, PR China

[c] Department of Advanced Materials Science, Faculty of Engineering, Kagawa University, 2217-20 Hayashi-cho, Takamatsu-shi, 761-0396 Japan

[d] Anhui Deli Household Glass Co., Ltd., Fengyang Gate Taiwan Industrial Park, Anhui 223121, PR China

*Author to whom correspondence should be addressed. E-mail: yezhu_1983@163.com

Abstract

This paper introduces one-dimensional $ZnNb_2O_6/KNbO_3$ hetero-nanostructures and one-dimensional $ZnNb_2O_6$ nanostructures. These nanostructures are synthesized via *in situ* topotactic structural transformation reaction using the tunnel structure $K_2Nb_2O_6$ filiform crystal as precursor. Firstly, Zn^{2+} ions intercalate into $K_2Nb_2O_6$ crystal by the exchange K^+ ions of $K_2Nb_2O_6$ crystal with Zn^{2+} in $Zn(NO_3)_2$ or $Zn(CH_3COO)_2$ aqueous solution, to form two different Zn^{2+}-exchanged samples, and then these Zn^{2+}-exchanged samples topotacticly transformed into one-dimensional $ZnNb_2O_6/KNbO_3$ hetero-nanostructures and $ZnNb_2O_6$ nanostructures during heat-treatment, respectively. The formation reaction and structure of these samples were characterized by X-ray diffraction (XRD), field-emission scanning electron microscopy (FE-SEM), transmission electron microscopy (TEM), selected-area electron diffraction (SAED), and energy-dispersive spectroscopy (EDS). Photocatalytic experiments showed that one-dimensional $ZnNb_2O_6/KNbO_3$ hetero-nanostructures and $ZnNb_2O_6$ nanostructures have excellent photocatalytic performance for the degradation of methylene blue (MB), rhodamine B (RhB), and methyl orange (MO).

Keywords: nanostructures, hetero-nanostructures, topotactic structural transformation, one-dimension, photocatalytic material, $ZnNb_2O_6$

Introduction

The soft chemical process is a useful and unique method for preparation and design of function inorganic materials.[1-3] This process typically comprises two steps: the first step is the preparation of a framework precursor with layered or tunnel structure and insertion of template ions or molecules into the interlayer space by ion-exchange reaction, and the second step is the transformation of the template-inserted precursor into a desired structure by the soft chemical method, such as solvothermal treatment, ion-exchange treatment and low temperature heat-treatment. The crystal structure of the product can be controlled by the used template, and the product particle morphology is dependent on the morphology of the used precursor. This method has been utilized for the synthesis and design of metal oxide and nanocomposite with controlled structure, morphology, and chemical composition.[4-6]

Chemical composition, structure, morphology, and grain size of semiconductor materials as photocatalysts are some key issues that influence the photocatalytic capability.[7-9] Because photocatalytic reactions are typically surface-based processes and the photocatalytic efficiency is closely related to the morphology and micro-structure of the material. One-dimensional (1D) nanostructures and hetero-nanostructures such as wires, belts and tubes have attracted considerable attention for photocatalytic applications due to their distinct electronic, optical and chemical properties, which differ from their bulk counterparts.[10-12]

Among all the semiconductor photocatalysts reported, some niobates showed certain photocatalytic performance, such as $KNbO_3$,[13] $NaNbO_3$,[14] $K_4Nb_6O_{17}$,[15] $CaNb_2O_6$,[16] pyrochlore type $K_2Nb_2O_6$,[17] $Sn_2Nb_2O_7$,[18] Nb^{4+} self-doped $K_4Nb_6O_{17}$,[19] $SnNb_2O_6$–graphene nanocomposite [20] and so on. $ZnNb_2O_6$, with a columbite structure, has received a great deal of attention due to its microwave dielectric, photoluminescence and photocatalytic properties.[21,22] Most studies have found that $ZnNb_2O_6$ show photocatalytic activity for water splitting and degradation of diverse organic pollutants.[22-24] Currently, its main synthesis approaches includes traditional solid-state,[21] sol-gel,[23] hydrothermal[24] and molten-salt method.[25] Until now, however, 1D nanostructures and hetero-nanostructures $ZnNb_2O_6$ have not been reported because these methods mentioned above are difficult to simultaneously control chemical composite, grain size, morphology and nanostructure.

In our previous study of controlling morphology and chemical composition, we used the layered structure titanate $H_{1.07}T_{1.73}O_4 \cdot nH_2O$ particles with plate-like morphology as precursor to prepare some plate-like particles ($BaTiO_3$, $Ba_{0.9}Ca_{0.1}TiO_3$, $Ba_{0.5}(Bi_{0.5}K_{0.5})_{0.5}TiO_3$) by the soft chemical process.[26, 27] In the soft chemical process, the layered structure of HTO precursor is transformed into the perovskite structure by an *in situ* topotactic transition reaction, and the precursor morphology is remained after the reaction. In this paper, therefore, an *in situ* topotactic structural transformation synthesis of 1D nanostructures $ZnNb_2O_6$ and hetero-nanostructures $ZnNb_2O_6/KNbO_3$ is described in detail and their formation reaction mechanism is clarified. In addition, the photocatalytic activities of these materials are discussed.

Experimental Section

Preparation of $K_2Nb_2O_6$ Precursor

The starting material of the tunnel structure potassium niobate $K_2Nb_2O_6{\cdot}nH_2O$ fibrous crystal was prepared using the method described in literature.[28] 5g of Nb_2O_5 and 30 mL of 3mol/L-KOH water solution were placed in a Teflon-lined, sealed stainless-steel vessel with an inner volume of 85 mL, and then hydrothermally treated at 200°C for 2 h under stirring conditions. After the hydrothermal treatment, a potassium hexaniobate clear solution was obtained. Potassium hexaniobate was precipitated out from this solution by adding the ethanol into the solution. The precipitate was filtered, washed with ethanol, and then dried at room temperature. 0.5 g of potassium hexaniobate and 30 mL of 0.5 mol/L-KOH water–ethanol (volume ratio = 1/1) solution were added into a Teflon-lined, sealed stainless-steel vessel with an inner volume of 85 mL, and then solvothermally treated at 230°C for 12 h under stirring conditions. After the solvothermal treatment, the tunnel structure $K_2Nb_2O_6{\cdot}nH_2O$ fibrous crystal sample was filtered, washed with distilled water, and then dried at room temperature.

Preparation of $ZnNb_2O_6$ and $ZnNb_2O_6/KNbO_3$

0.5g of $K_2Nb_2O_6{\cdot}nH_2O$ samples were respectively put into 200 mL of 0.5 $mol{\cdot}L^{-1}$-$Zn(CH_3COO)_2$ and 0.5 $mol{\cdot}L^{-1}$-$Zn(NO_3)_2$ aqueous solution, then stirred and ion-exchanged for 24h at room temperature. The ion-exchange treatment was performed twice for the complete exchange. After ion-exchange, the products were filtered, washed with distilled water, and dried at room temperature. The

Zn^{2+}-exchanged samples were obtained. Finally, the Zn^{2+}-exchanged samples were heat-treated at 570°C for 2h, to respectively obtain $ZnNb_2O_6$ and $ZnNb_2O_6/KNbO_3$ samples.

Physical Analysis.

The crystal structure of the sample was investigated using a powder X-ray diffractometer (Shimadzu, Model XRD-6100) with Cu Kα (λ = 0.15418 nm) radiation. The size and morphology of the particles were observed using scanning electron microscopy (SEM) (Hitachi, Model S-900). Transmission electron microscopy (TEM) observation and selected-area electron diffraction (SAED) were performed on a JEOL Model JEM-3010 system at 300 kV, and the powder sample was supported on a micro grid. Chemical composition analysis was carried out with energy dispersive spectroscopy (EDS) (JEOL Model JED-2300T) on the TEM system. Thermo gravimetric and differential thermal analyses (TG-DTA) were conducted on a DTG-60Hthermogravimetric analyzer (SHIMADZU). UV–vis absorption spectra were recorded on a UV/vis/NIR Spectrophotometer (LAMBDA950, PerkinElmer).

The photocatalytic performance of samples were evaluated by degradation of methylene blue (MB), rhodamine B (RhB), and methyl orange (MO) under xenon lamp irradiation. In each experiment, 50 mg of samples were added into the solution (50 mL, 10 $mg \cdot L^{-1}$). The suspensions were magnetically stirred in dark for 40min to ensure the establishment of an adsorption–desorption equilibrium. Then, the solution was exposed to the lamp irradiation under magnetic stirring. At different irradiation time intervals, 6 mL of the solution was collected with centrifugation. The

concentration of the remnant dye in the collected solution was monitored by UV–vis spectroscopy (Unico UV-2600) each 5 or 10 min.

Result and Discussion

Zn^{2+}-exchange of Tunnel Structure $K_2Nb_2O_6$

In the previous study,[28] we have reported a tunnel structure $K_2Nb_2O_6$, which is composed of NbO_6 double chains and KO_6 octahedron layers with the K^+ occupying the tunnel sites, and a single crystal with filiform shape. Similar to the most metal oxides with tunnel structure, e.g. zeolites, tunnel structure manganese oxides,[29, 30] layered niobates of KNb_3O_8 and $K_4Nb_6O_{17}$,[31, 32] K^+ ions in the tunnel structure $K_2Nb_2O_6$ can be exchanged with other cation by ion-exchange treatment.

Fig.1 is the XRD patterns of samples obtained by the ion-exchange of $K_2Nb_2O_6$ with Zn^{2+} ion. The precursor $K_2Nb_2O_6$ possessed a characteristic peak of tunnel structure at $2\theta=10^o$ nearby and the fine crystallinity (Fig. 1a). When the $K_2Nb_2O_6$ precursor was respectively treated by ion-exchange in 0.5 $mol\cdot L^{-1}$-$Zn(NO_3)_2$ and 0.5 $mol\cdot L^{-1}$-$Zn(CH_3COO)_2$ aqueous solution, the Zn^{2+}-exchanged samples were formed (Fig. 1b and c). Although the crystallinity of Zn^{2+}-exchanged samples decreased, they retained the tunnel structure because of existing the characteristic peak at $2\theta=10^o$ nearby in their XRD patterns (Fig. 1b and c). The FE-SEM result reveals that the Zn^{2+}-exchanged samples all retained the filiform morphology of precursor after the Zn^{2+}-exchange process (Fig. 2).

The chemical composite analysis result revealed that the mole ratio of K, Zn and Nb was 0.4/0.6/1 in the Zn^{2+}-exchanged sample obtained in $Zn(CH_3COO)_2$ aqueous

solution. This indicated that K^+ ions in the $K_2Nb_2O_6$ precursor cannot be completely exchanged with Zn^{2+} ions in $Zn(CH_3COO)_2$ aqueous solution. This is similar to the our previous report that K^+ ions in the $K_2Nb_2O_6$ precursor cannot be completely exchanged by Li^+ ions in LiCl aqueous solution.[28] In the Zn^{2+}-exchanged sample obtained from $Zn(NO_3)_2$ aqueous solution, however, no K component is detected, and the mole ratio of Zn and Nb is 0.99/1. This reason is that the 0.5 $mol \cdot L^{-1}$-$Zn(CH_3COO)_2$ aqueous solution close to neutral (pH=6.7 by actual measurement), whereas the $Zn(NO_3)_2$ aqueous solution is acidity (pH=4.1 by actual measurement), meanwhile, the KO_6 octahedral layers in the tunnel structural framework is not steady and easily reacted with H^+ in the acid environment[28], resulting in the KO_6 octahedral layers dissolved out. These results suggested that the acid-base property in the ion-exchange system have an effect on the K^+ exchange process of $K_2Nb_2O_6$. But Zn^{2+} ion can react with OH^-, forming $Zn(OH)_2$ precipitate at alkaline condition, we did not systematically research the pH effect over Zn^{2+}-exchange reaction system.

Structure Transition Reaction

The tunnel structure $K_2Nb_2O_6$ filiform crystal can topotacticly transform into the pure perovskite $KNbO_3$ (noted as $KNbO_3$-HT) filiform crystal via heat-treatment (Fig.3a).[28] Therefore, we heat-treated the Zn^{2+}-exchanged samples according to their TG-DTA curves (Fig. 4). Two types of Zn^{2+}-exchanged samples obtained respectively in the $Zn(CH_3COO)_2$ and $Zn(NO_3)_2$ solution showed the different exothermic peaks without weight loss around 528 and 560 °C, which correspond to the phase

transformations. Thus, the heat-treatments were processed at 570 ^{o}C.

Figure 3 presented the XRD patterns of the heat-treated samples. It is found that the mixed phase of columbite $ZnNb_2O_6$ (JCPDS File No. 37-1371) and perovskite $KNbO_3$ (JCPDS File No.32-0822) were formed after the heat-treatment of the Zn^{2+}-exchanged sample obtained in $Zn(CH_3COO)_2$ solution (Fig. 3b). While the Zn^{2+}-exchanged sample obtained in $Zn(NO_3)_2$ solution transformed into a pure columbite phase $ZnNb_2O_6$ (noted as $ZnNb_2O_6$-HT)(JCPDS File No. 37-1371) after the heat-treatment (Fig. 3c). The chemical composite analysis indicated that the mole ratios of K, Zn and Nb are the same in samples before and after the heat-treatment. Above results suggested that the Zn^{2+}-exchanged niobate samples can transform into the columbite $ZnNb_2O_6$ by soft chemical heat-treatment process.

The FE-SEM images revealed that the mixed phase sample and the $ZnNb_2O_6$-HT sample still keep the filamentous morphology of precursor after the heat-treatment (Fig. 5). It can be clearly seen that the mixed phase filamentous particle was constructed from nanocube with a size of ~20 nm (Fig. 5a), meaning a polycrystalline. And the $ZnNb_2O_6$-HT filamentous particle was also a polycrystalline which consists of the needle-like nanocrystals with a size of ~10 nm (Fig. 5b). Nevertheless, the solid-state method can only synthesized $ZnNb_2O_6$ sample ($ZnNb_2O_6$-Solid) with sphere morphology and a size of 500 nm (Fig. 5c). These results suggested that the filamentous morphology of products depends on the filiform morphology of the tunnel structure $K_2Nb_2O_6$ precursor. Therefore, the transformation reactions from tunnel structure $K_2Nb_2O_6$ to columbite structure $ZnNb_2O_6$ and perovskite structure

$KNbO_3$ were topotactic structural transition reactions.

Nanostructure Study

Similar to the SEM results, the TEM images also showed that the mixed phase sample and the $ZnNb_2O_6$-HT sample have filamentous shapes (Fig. 6). In HRTEM image of the mixed phase sample (Fig. 6b), it can be observed the lattice image of $ZnNb_2O_6$ structure with lattice spacing of $d_{(002)}$ = 0.368 and the lattice image of $KNbO_3$ structure with lattice spacing of $d_{(110)}$ =0.286, in addition a grain boundary existing between the (002) plane of the $ZnNb_2O_6$ phase and the (110) plane of the $KNbO_3$ phase. It was demonstrated that the columbite $ZnNb_2O_6$ and the perovskite $KNbO_3$ phases coexisted in one filamentous particle. Therefore, it can be confirmed that the mixed phase polycrystalline fiber was a $ZnNb_2O_6/KNbO_3$ nanocomposite (noted as $ZnNb_2O_6/KNbO_3$-HT), meaning a 1-D hetero-nanostructures.

It was interesting that although the $ZnNb_2O_6$-HT sample was a polycrystalline fiber, it showed a SAED pattern similar to a $ZnNb_2O_6$ single crystal (Fig. 6c). In SAED pattern of $ZnNb_2O_6$-HT sample (Fig. 6d), the d-values of diffraction spots were 0.254 and 0.369 nm, which corresponded to the (440) and (002) planes of the $ZnNb_2O_6$ structure, respectively. This indicated that all the needle-like nanocrystals in each fiber were arranged in the same crystal-axis orientation, meaning perfectly oriented polycrystalline fiber, and the fiber-axis direction directs to the [110]-axis direction of the $ZnNb_2O_6$ structure. In our previous report[28], the fiber axis direction of precursor was [010]-axis direction of the $K_2Nb_2O_6$ tunnel structure. It implied that the [010]-axis direction of $K_2Nb_2O_6$ tunnel structure transformed into the [110]-axis

direction of $ZnNb_2O_6$ columbite structure and there was a corresponding relation between them. Therefore, the polycrystalline $ZnNb_2O_6$-HT fiber was a 1-D nanostructures with [110]-crystal-axis orientation.

The above results revealed that $ZnNb_2O_6/KNbO_3$ 1-D hetero-nanostructures and $ZnNb_2O_6$ 1-D nanostructures with crystal-axis orientation can be fabricated by the topotactic structural transformation of the tunnel structure $K_2Nb_2O_6$ fiber.

Formation Reaction Mechanism

A schematic representation of the formation mechanism of one-dimensional $ZnNb_2O_6$ nanostructures and $ZnNb_2O_6/KNbO_3$ hetero-nanostructures in the two-step soft chemical process was given in Figure 7. When the ion-exchange treatment of tunnel structure $K_2Nb_2O_6$ filiform crystal was operated in near neutral $Zn(CH_3COO)_2$ solution, firstly Zn^{2+} ions intercalate into $K_2Nb_2O_6$ crystal by the exchange K^+ in tunnel pathway of $K_2Nb_2O_6$ crystal with Zn^{2+} ions, and then these Zn^{2+} ions and KO_6 layer react with NbO_6 double chains to form the $ZnNb_2O_6/KNbO_3$ composite phase by an *in situ* topotactic structural transformation reaction during heat-treatment.[27, 29] Nevertheless, in $Zn(NO_3)_2$ solution, not only K^+ ions in tunnel but also in KO_6 layer of $K_2Nb_2O_6$ crystal were exchanged out by Zn^{2+} ions. It is well known that the $Zn(NO_3)_2$ aqueous solution presents acidity and the KO_6 layer of $K_2Nb_2O_6$ crystal is not steady in this acidic system and easily reacted with H^+ ions and dissolved, leading that the Zn^{2+} ions filled among the NbO_6 double chains. In the heat-treatment process, the Zn^{2+} ions reacted with the NbO_6 double chains and formed the pure $ZnNb_2O_6$ phase by *in situ* topotactic structural transformation reaction. Since the topotactic

structural transformation reaction occurs in ion-exchanged sample, $ZnNb_2O_6/KNbO_3$ hetero-nanostructures and $ZnNb_2O_6$ nanostructures, as shown in Figure 5, were respectively formed and all remained the one-dimensional fibrous shape of precursor. The mechanism described above suggests that the acid-base property of the system during ion-exchange can determine the selective formation of 1-D $ZnNb_2O_6$ nanostructures and 1-D $ZnNb_2O_6/KNbO_3$ hetero-nanostructures.

UV-Vis Absorption Spectra Analysis

Figure 8a showed the UV-vis diffuse reflectance spectra of samples. It can be noticed that all of the samples exhibited absorption bands in the UV light region. The sphere $ZnNb_2O_6$-Solid sample showed strong absorption in the UV-light regions (250−320 nm). The filiform $ZnNb_2O_6$-HT sample presented slight red-shift of absorption edge (270−350 nm) relative to $ZnNb_2O_6$-Solid sample, and its color is the light orange, but $ZnNb_2O_6$-Solid sample presents the white color (Fig. 8b and c). The reason is that the nanocrystal size of $ZnNb_2O_6$-HT sample is smaller than that of $ZnNb_2O_6$-Solid sample (Fig. 5b and c) and the nanocrystal in $ZnNb_2O_6$-HT sample possess a higher internal stress of the nanocrystals relative to that of $ZnNb_2O_6$-Solid sample, resulting in a red shift of the absorption edge.[33] Theoretically, although a generally received opinion is that the ubiquitous blue shift of the absorption edge of nanocrystals is the result of the quantum size effect owing to the downsized crystals. The absorption of $KNbO_3$-HT filamentous crystal sample was in the UV-light regions of 280~380 nm, but the filiform $ZnNb_2O_6/KNbO_3$-HT sample showed the step-like absorption curve within wavelength regions of 250~400 nm, which was related to its

nanocomposite structure.[34] And its color was also the light orange (Fig. 8d).The differences in optical absorption of the different samples may be ascribed to their filiform shape and nanostructure.[7-9]

Photocatalytic Performance

Figure 9 displayed the temporal evolution of the spectral changes during the photodegradation of RhB over $ZnNb_2O_6$-Solid sample under UV-light illumination. It can be seen that the absorbance of RhB at the maximum absorption wavelength (551 nm) was gradually decreased with the prolongation of the irradiation time, which was because the chromophoric structure of the dye was destroyed. After 100 min, the major absorption band displayed blue-shift, indicating the de-ethylation of RhB molecules.[35]

Figure 10 showed the photocatalytic performance (C/C_0) versus UV-light irradiation time of samples for the degradation of methylene blue (MB), Rhodamine B (RhB), and methyl orange (MO). The $KNbO_3$-HT sample and the $ZnNb_2O_6$-Solid sample displayed the degradation efficiency of about 80% for MB after UV-light irradiation for 40min. Nevertheless, the $ZnNb_2O_6$-HT sample took about 10 min to reach the degradation efficiency of about 88% for MB. It is surprise that the $ZnNb_2O_6/KNbO_3$-HT sample need only 5 min to reach to the degradation efficiency of about 90% for MB. It was found that the photocatalytic activities of both $ZnNb_2O_6$-HT and $ZnNb_2O_6/KNbO_3$-HT sample were superior to that of $KNbO_3$-HT and $ZnNb_2O_6$-Solid samples for the degradation of MB. The similar results were also observed in the UV-light degradation process of RhB and MO (Fig. 9b and c). The

reason is that the smaller the particle size, the higher the photocatalytic efficiency.[7,8] These small nanocrystals in $ZnNb_2O_6$-HT and $ZnNb_2O_6/KNbO_3$-HT samples are generally beneficial for surface-based photocatalysis. More importantly, the hetero-nanostructure of $ZnNb_2O_6/KNbO_3$-HT samples may be responsible for its highest photocatalytic activity because the synergetic effect on photocatalytic performance may occur in the grain boundary between $ZnNb_2O_6$ nanocrystal and $KNbO_3$ nanocrystal in 1D hetero-nanostructures.[9, 36, 37] Herein, we cannot give its band gap structures for discussing the detailed photocatalytic mechanism, because our experimental conditions are restricted.

Conclusion

The 1-D $ZnNb_2O_6/KNbO_3$ hetero-nanostructures and 1-D $ZnNb_2O_6$ nanostructures were successfully synthesized by *in situ* structural transformation reaction. Firstly Zn^{2+} ions intercalate into $K_2Nb_2O_6$ crystal by the exchange K^+ ions in of $K_2Nb_2O_6$ crystal with Zn^{2+} in $Zn(CH_3COO)_2$ or $Zn(NO_3)_2$ aqueous solution, respectively forming two types of Zn^{2+}-exchanged samples. And then these Zn^{2+}-exchanged samples topotacticly transformed into 1-D $ZnNb_2O_6/KNbO_3$ hetero-nanostructures and 1-D $ZnNb_2O_6$ nanostructures during heat-treatment, respectively. These Zn^{2+} ions and KO_6 layer react with NbO_6 double chains to form the $ZnNb_2O_6$ and $KNbO_3$ phase by an *in situ* topotactic structural transformation reaction during heat-treatment. 1-D $ZnNb_2O_6/KNbO_3$ hetero-nanostructures and 1-D $ZnNb_2O_6$ nanostructures display excellent photocatalytic performance for the degradation MB, RhB and MO under ultraviolet irradiation. It is believed that the

topotactic structural transformation process is an efficient method for designing and preparing other new types of nanostructures or hetero-nanostructures functional materials.

Acknowledgments

This work was financially supported by the Natural Science Basic Research Plan in Shaanxi Province of China (Program No.2013JQ6012), the China Postdoctoral Science Foundation (Program No.2013M542314), the research starting foundation from Shaanxi University of Science and Technology (BJ12-22), the Natural Science Foundation of China (NO. 21173003& No. 51472153), and Innovation Team Assistance Foundation of Shaanxi Province (Grant No. 2013KCT-06).

References

1 Q. Feng, M. Hirasawa and K. Yanagisawa, *Chem. Mater.*, 2001, **13**, 290.

2 Q. Feng, C. Honbu, K. Yanagisawa and N. Yamasaki, *Chem. Lett.*, 1998, 757.

3 Q. Feng, C. Honbu, K. Yanagisawa and N. Yamasaki, *Chem. Mater.*, 1999, **11**, 2444.

4 J. Gopalakrishnan, S. Uma, K. K.Rangan and N. S. P. Bhuvanesh, *P. Indian AS-Chem. Sci.*, 1994, **106**, 609.

5 Y. Komori, Y. Sugahara and K. Kuroda, *Chem. Mater.*, 1999, **11**, 3.

6 T. Sasaki, M. Watanabe, Y. Fujiki and Y. Kitami, *Chem. Mater.*, 1994, **6**, 1749.

7 Z. Jiang, Y. Tang, Q. Tay, Y. Zhang, O. Malyi, D. Wang, J. Deng, H. Zhou, X. Chen and Z. Chen, *Adv. Energy Mater.*, 2013,**3**, 1368.

8 A. Kubacka, M. Fernandez and G. Colon, *Chem. Rev.*, 2011, **112**, 1555.

9 H. Tong, S. Ouyang, Y. Bi, N. Umezawa, M. Oshikiri and J. Ye, *Adv. Mater.*, 2012, **24**, 229.

10 Y. Bi and J. Ye, *Chem. Eur. J.*, 2010, **16**, 10327.

11 Y. Bi and J. Ye, *Chem. Commun.*, 2009, **43**, 6551.

12 S. Chatterjee, K. Bhattacharyya, P. Ayyub and A. Tyagi, *J. Phys. Chem. C*, 2010,**114**, 9424.

13 H. Shi, X. Li, D. Wang, Y. Yuan, Z. Zou and J.Ye, *Catal. Lett.*, 2009, **132**, 205.

14 Q. Ding, Y. Yuan, X. Xiong, R. Li, H. Huang, Z. Li, T. Yu, Z. Zou and S. Yang, *J. Phys. Chem. C*, 2008, **112**, 18846.

15 H. Hayashi, Y. Hakuta and Y.Kurata, *J. Mater. Chem.*, 2004, **14**, 2046.

16 Y. Zhang, C. Liu, G. Pang, S. Jiao, S. Zhu, D. Wang, D. Liang and S. Feng, *Eur. J. Inorg. Chem.*, 2010, **8**, 1275.

17 J. Wu, C. Zhou, Y. Zhao, L. Shang, T. Bian, L. Shao, F. Shi, L. Wu, C. Tung and T. Zhang, *Chin. J. Chem.*, 2014, **32**, 485-490.

18 C. Zhou, Y. Zhao, T. Bian, L. Shang, H. Yu, L. Wu, C. Tung and T. Zhang, *Chem. Commun.*, 2013, **49**, 9872-9874 2008.

19 C. Zhou, Y. Zhao, L. Shang, Y. Cao, L. Wu, C. Tung and T. Zhang, *Chem. Commun.*, 2014, **50**, 9554-9556.

20 L. Yuan, M. Yang and Y. Xu, *Nanoscale*, 2014, **6**, 6335-6345.

21 S. Ji, S. Choi, J. Jang, E. Kim and J. Lee, *J. Phys. Chem. C*, 2009, **113**, 17824.

22 W. Wu, S. Liang, Z. Ding, H. Zheng and L. Wu, *Solid State Sci.*, 2011, **13**, 2019.

23 Y. Hsiao, T. Fang and L. Ji, *Mater. Lett.*, 2010, **64**, 2563.

24 J. Dai, C. Zhang, L. Shi, W. Song, P. Wu and X. Huang, *Ceram. Int.*, 2012, **38**, 1211.

25 L. Guo, J. Dai, J. Tian, Z. Zhu and T. He, *Mater. Res. Bull.*, 2007, **42**, 2013.

26 X. Kong, Y. Ishikawa, K. Shinagawa and Q. Feng, *J. Am. Ceram. Soc.*, 2011, **94**, 3716.

27 X. Kong, D. Hu, Y. Ishikawa, Y. Tanaka and Q. Feng, *Chem. Mater.*, 2011, **23**, 3978.

28 X. Kong, D. Hu, P. Wen, T. Ishii, Y. Tanaka and Q. Feng, *Dalton Trans.*, 2013, **42**, 7699.

29 Q. Feng, H. Kanoh and K.Ooi, *J. Mater. Chem.*, 1999, **9**, 319.

30 P. Misaelides, *Microporous Mesoporous Mater.*, 2011, **144**, 15.

31 M. Bizeto, A. Shiguihara and V. Constantino, *J. Mater. Chem.*, 2009, **19**, 2512.

32 H. Lin, T. Lee and C. Sie, *Int. J. Hydrogen. Energy.*, 2008, **33**, 4055.

33 J. Huang, C. Xia, L. Cao and X. Zeng, *Mater. Sci. Eng. B*, 2008, **150**,187.

34 G. Tan, L. Zhang, H. Ren, S. Wei, J. Huang and A. Xia, *ACS Appl. Mater. Inter.*, 2013, **5**, 5186.

35 L. Zhou, W. Wang, L. Zhang, H. Xu, W. Zhu, *J. Phys. Chem. C*, 2007, **111**, 13659.

36 W. Lu, J. Xiang, B. Timko, Y. Wu and C. M. Lieber, *Proc. Natl. Acad. Sci. USA*, 2005, **102**, 10046.

37 J. Xiang, W. Lu, Y. Hu, Y. Wu, H. Yan and C. M. Lieber, *Nature*, 2006, **441**, 489.

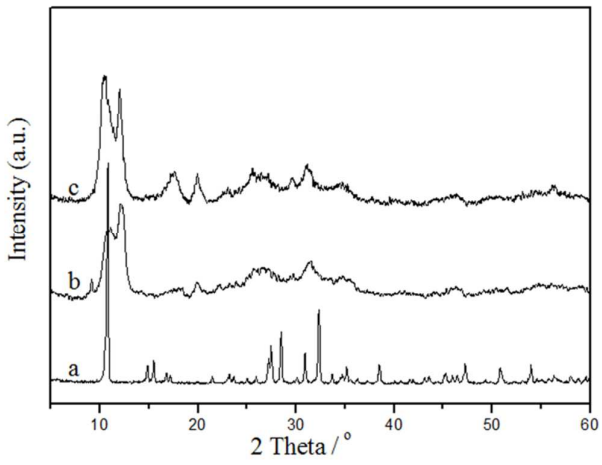

Fig. 1. XRD patterns of (a) the tunnel structure $K_2Nb_2O_6$ and the Zn^{2+}-exchanged samples obtained in (b) $Zn(NO_3)_2$ and (c) $Zn(CH_3COO)_2$ solution, respectively.

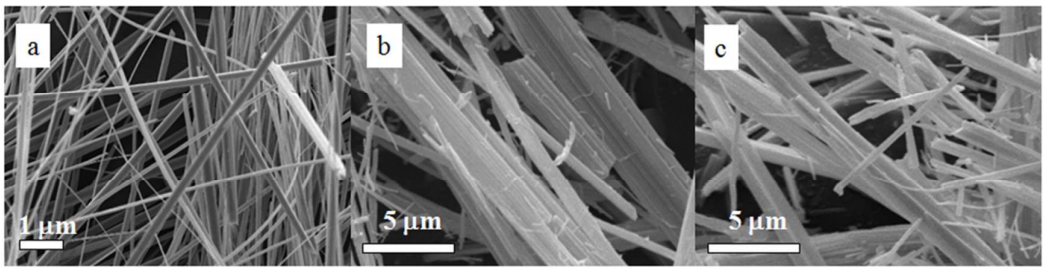

Fig. 2. FE-SEM images of (a) the tunnel structure $K_2Nb_2O_6$ niobate and the Zn^{2+}-exchanged samples obtained in (b) $Zn(NO_3)_2$ and (c) $Zn(CH_3COO)_2$ solution, respectively.

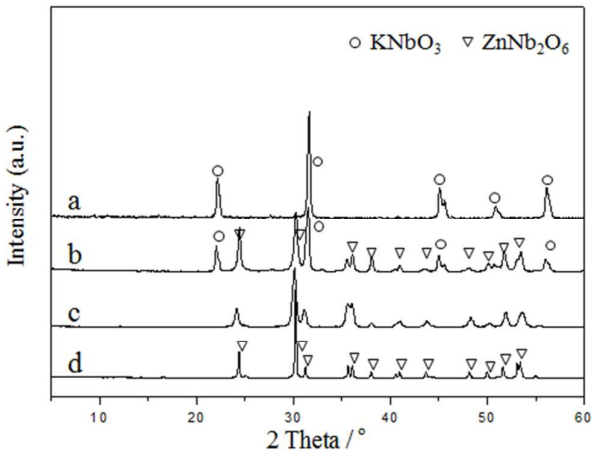

Fig. 3. XRD patterns of (a) the $KNbO_3$ sample obtained by heat-treating the tunnel structure $K_2Nb_2O_6$ sample, the samples obtained by heat-treating the Zn^{2+}-exchanged samples from (b) $Zn(CH_3COO)_2$ and (c) $Zn(NO_3)_2$ solution, and (d) the $ZnNb_2O_6$ sample obtained by solid-state method.

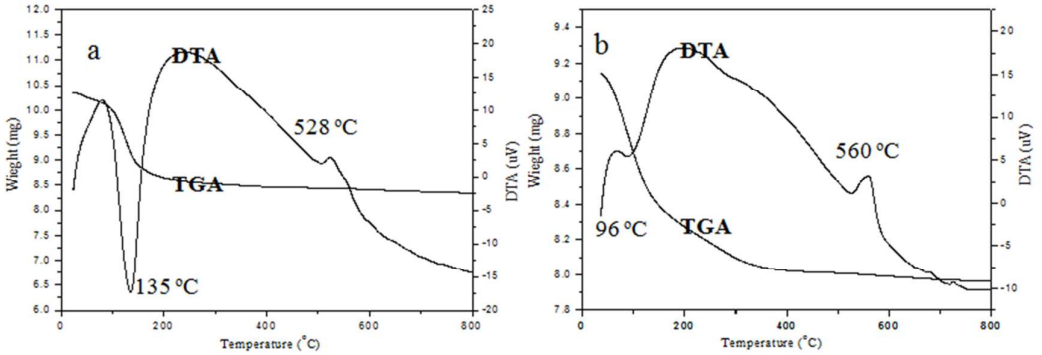

Fig. 4. TG-DTA curves of the Zn^{2+}-exchanged samples from (a) $Zn(CH_3COO)_2$ and (b) $Zn(NO_3)_2$ solution, respectively.

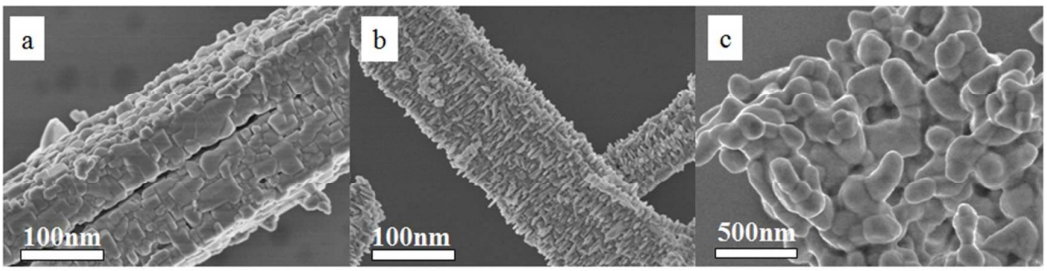

Fig. 5. FE-SEM images of the samples obtained by heat-treating the Zn^{2+}-exchanged samples from (a) $Zn(NO_3)_2$ and (b) $Zn(CH_3COO)_2$ solution, and (c) the $ZnNb_2O_6$ sample obtained by solid-state method.

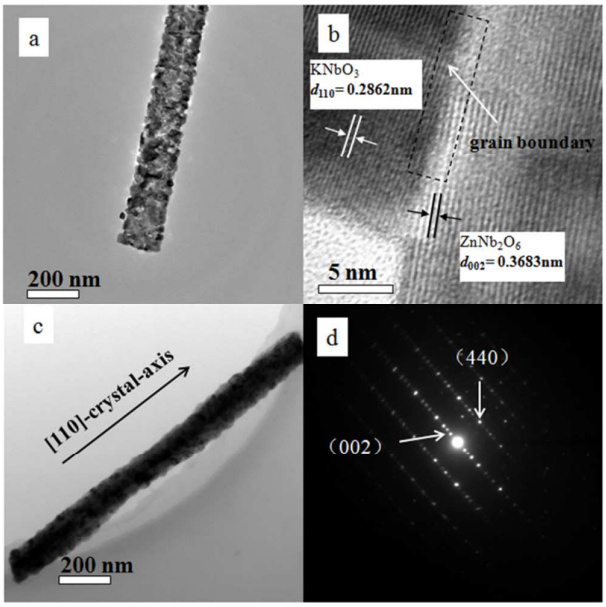

Fig. 6. TEM (a) and HRTEM image (b) of the samples obtained by heat-treating the Zn^{2+}-exchanged samples from $Zn(CH_3COO)_2$ solution, and TEM image(c) and SAED pattern (d) of the samples obtained by heat-treating the Zn^{2+}-exchanged samples from $Zn(NO_3)_2$ solution.

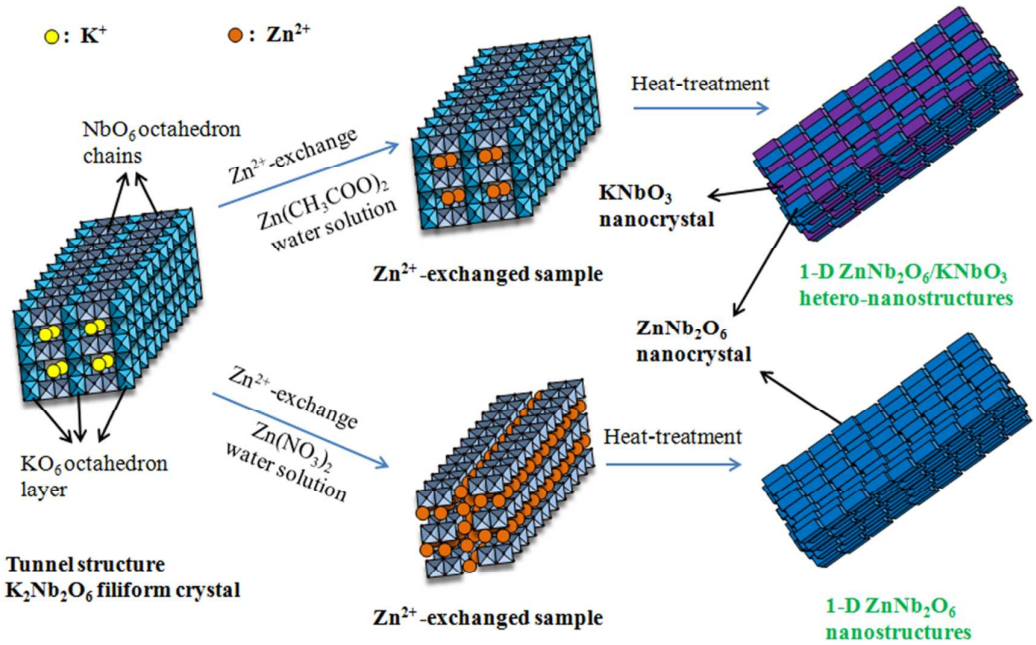

Fig. 7. Formation mechanism of one-dimensional $ZnNb_2O_6$ nanostructures and

$ZnNb_2O_6/KNbO_3$ hetero-nanostructures from $K_2Nb_2O_6$.

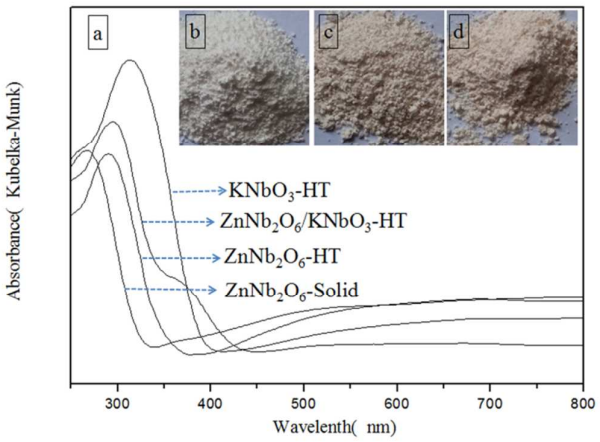

Fig. 8. UV-vis diffuse reflectance spectra (a) and photos of (b) $ZnNb_2O_6$-Solid sample, (c) $ZnNb_2O_6$-HT sample, and (d) $ZnNb_2O_6/KNbO_3$-HT sample.

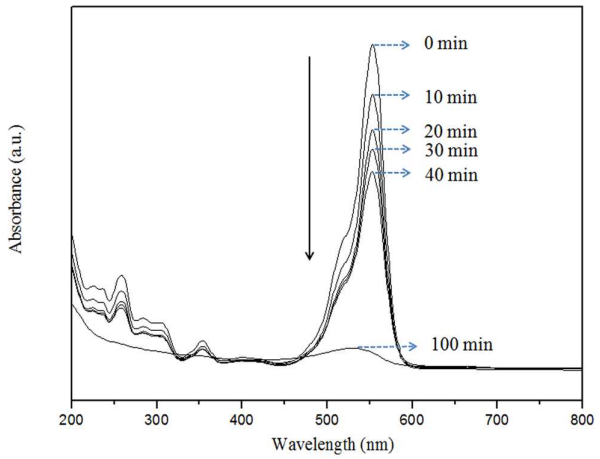

Fig. 9. Time-dependent UV-vis absorption spectra of the RhB solution in the presence of the $ZnNb_2O_6$-Solid sample.

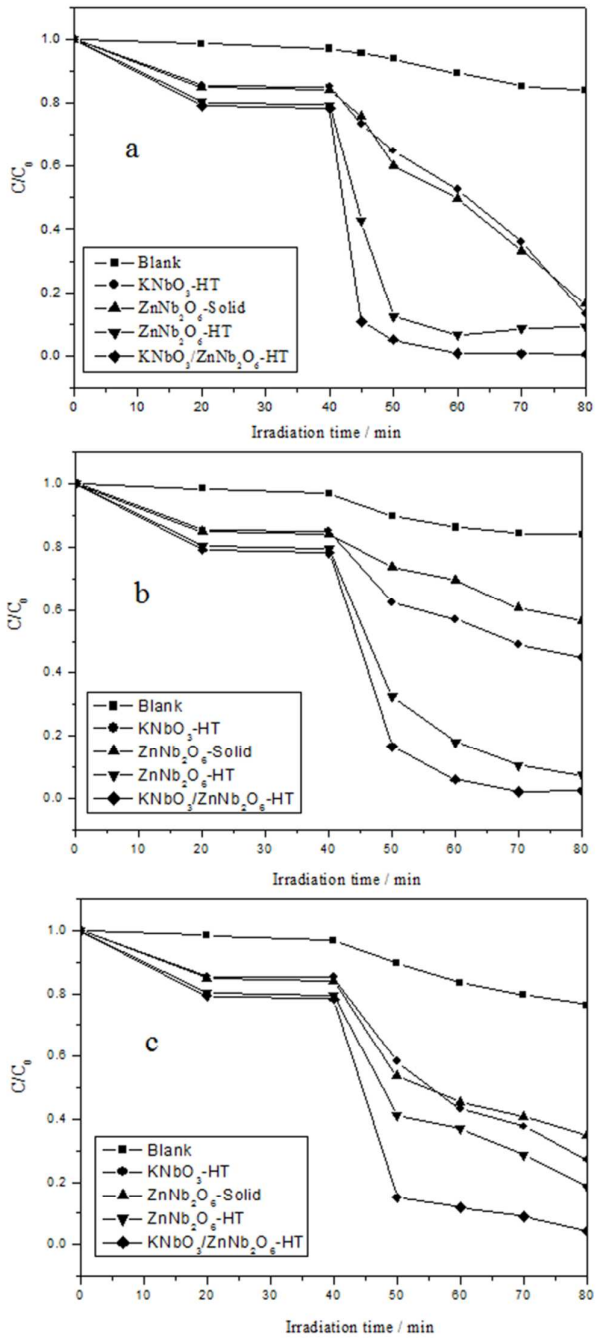

Fig. 10. Photocatalytic degradation of (a) MB, (b) RhB , and (c) MO under UV-light irradiation using the $KNbO_3$-HT sample, the $ZnNb_2O_6$-Solid sample, the $ZnNb_2O_6$-HT, and the $ZnNb_2O_6$/$KNbO_3$-HT sample.

Title: Topotactic synthesis and photocatalytic performance of one-dimensional $ZnNb_2O_6$ nanostructures and one-dimensional $ZnNb_2O_6/KNbO_3$ hetero-nanostructures

Author: Xingang Kong*, Zhanglin Guo, Puhong Wen, Liyun Cao, Jianfeng Huang, Cuiyan Li, Jie Fei, Fen Wang, Qi Feng

The table of contents entry: Zn^{2+} ions intercalate into $K_2Nb_2O_6$ crystal by exchange K^+ ions of $K_2Nb_2O_6$ crystal with Zn^{2+} in $Zn(NO_3)_2$ or $Zn(CH_3COO)_2$ aqueous solution, forming two different Zn^{2+}-exchanged samples, and then these Zn^{2+}-exchanged samples topotacticly transformed into one-dimensional $ZnNb_2O_6/KNbO_3$ hetero-nanostructures and $ZnNb_2O_6$ nanostructures during heat-treatment, respectively.

ToC figure :